DIRECTIONAL SOLIDIFICATION OF EUTECTIC ALLOYS AND PARTICULATE METAL MATRIX COMPOSITES DURING PARABOLIC FLIGHTS

D.M. Stefanescu, The University of Alabama, Tuscaloosa, AL 35487, USA
and
P.A. Curreri, NASA-Marshall Space Flight Center, Alabama 35812, USA

ABSTRACT

The advantages and disadvantages of directional solidification on parabolic trajectories are discussed as well as the influence of low-gravity solidification on interface stability, interlamellar spacing in eutectics and dendritic arm spacing. Behavior of insoluble particles at the solid-liquid interface is also analyzed. Experimental results on Fe-C, Fe-VC and Al-SiC systems are provided and explained.

1. INTRODUCTION

There is no question that microgravity experimentation has become an exciting new area for scientists and engineers alike due to the recent accessibility of extraterrestrial space. It has many promises and only one obvious drawback, which is the high cost involved in this type of experimentation. Directional solidification (DS) associated with an aircraft flying parabolic trajectories has emerged as an excellent low-cost experimental method for the study of solidification of alloys in simulated low gravity (low-g) experiments. Other advantages of this method are the access of the experimentor to the experiment during the totality of the experimental cycle and the

multiple number of parabolas which can be performed in a single flight. As main disadvantages, we can list the rather limited duration of the low-g periods (20-30 seconds) as well as the frequent transition from low-g to high-g resulting in transitory phenomena during solidification. The relative position of directional solidification on parabolic trajectories (DSPT) with respect to other available low-g experimental methods is summarized in Fig. 1 [1].

The present paper is an analysis of a number of DSPT experiments having both scientific and practical interest, performed by The University of Alabama in conjunction with NASA and different industrial and academic organizations. Four different subjects are covered, as follows:

1. Nucleation and grain multiplication in stable Fe-C alloys (gray cast iron).
2. Interface stability in Fe-C alloys
3. Interphase spacing in Fe-C alloys.
4. Insoluble particles behavior at the liquid/solid interface in Fe-C alloys, in-situ Fe-VC composites and in Al-SiC metal matrix composites.

2. PARAMETRIC ANALYSIS

The main scientific objective of low-g solidification experiments is to explain morphological changes at the solidifying interface in the light of fluid mechanics. This type of analysis requires first identifying and separating gravity-induced transport mechanisms from gravity-independent mechanisms as shown below [2]:

Gravity-induced transport processes:

- Density induced buoyancy and sedimentation.
- Natural convection induced by density variations due to temperature, $\rho(T)$, and composition, $\rho(C)$.

Gravity-independent transport process

- Convection caused by specific volume differnces between liquid and solid
- Diffusion.
- Marangoni convection induced by surface tension variation due to temperature, $\gamma(T)$, and composition $\gamma(C)$.

The second step consists in rationalizing the effects of suppression of gravity-induced transport processes via low-g experimentation on growth kinetics (interface stability and interphase spacing), nucleation kinetics and immiscible particle behavior at the interface.

2.1. Interface Stability: The well known condition for plane front solidification in the presence of convection [3,4] can be written as:

$$\frac{G}{R} \geq \frac{m}{D} C_o \, k_{ef}(1-f_s)^{k_{ef}-1} \frac{1-k}{k}$$

where G: temperature gradient in the liquid

R: solidification rate

m: slope of the liquidus line

C_0: initial concentration of solute

D: diffusivity in the melt

k: equilibrium partition coefficient

f_s: fraction of solid

$$k_{ef} = \frac{k}{k + (1-k) \exp(- R\delta_c/D)} \qquad (2)$$

δ_c: thickness of solutal boundary layer

Assuming a given system (m, k, C_0 constants) and a given experimental set-up (R constant), the variables which need to be considered when changing the gravity level, i.e. the convection level, are G, δ_c and D.

Let us consider first the temperature gradient in the liquid at the interface. As shown in Fig. 2, a thermal boundary layer, δ_T can be defined ahead of the interface which can be calculated from:

$$G = \left.\frac{dT}{dx}\right|_{x=0} = \frac{T_i - T_b}{\delta_T} \qquad (3)$$

where T_i: interface temperature

T_b: bulk temperature in the liquid

When the convection level is decreased, as when changing from high-g to low-g, δ_T increases and G decreases. This is equivalent to a destabilizing influence. In other words, decreasing the gravity level should result in interface instability.

The role of convection on the solutal boundary layer, δ_c, is shown in Fig. 3. It can be seen that as the level of convection increases, δ_c decreases and becomes zero when complete mixing is reached. It follows that decreasing the gravity level, which reduces

the natural convection, results in an increase in δ_c. Equation (2) implies correlations between k_{ef} and δ_c as shown in Table 1.

Using equation (1) it can be calculated that for all but large f_s and k, $(G/R)_{g=1} < (G/R)_{g=0}$, which means that in terms of the solute boundary layer, decreasing the gravity level increases interface stability (Figure 4). Consequently, although convection (high-g) decreases both δ_T and δ_c, the overall result on interface stability depends on the relative values of these boundary layers, since they act in opposite directions. In any event, when alloys with low solute content are used, the predominant influence is that of thermal convection, i.e., high-g has a stabilizing effect.

The combined influence of δ_T and δ_c can be rationalized in terms of a density driven convection boundary layer, δ_l. The driving force within this layer is the velocity gradient given by Newton's law:

$$\frac{\delta V}{\delta t} = \frac{\eta}{\rho} \frac{\delta^2 V}{\delta x^2} \qquad (4)$$

where η: viscosity

ρ: density.

Analysis along these lines shown schematically in Fig. 5 for solidification parallel to the gravity vectors indicates that an unstable density layer (negative density gradient) can occur ahead of the interface (Fig 5b).

Finally, the contribution of diffusivity, D, in eq. (1) must be discussed. According to ref. [5], measurements of diffisivity on Earth will in fact result in:

$$D_{ef(high-g)} = D_{true} + D_{wall} + D_{convection} \quad (5)$$

while in a low gravity environment will result in:

$$D_{ef(low-g)} = D_{true} + D_{wall} \text{ or } D_{ef(low-g)} < D_{ef(high-g)} \quad (6)$$

Indeed, experiments performed on Spacelab-1 [6] have shown that the liquid diffusivity measured for self-diffusion of liquid Sn at 10^{-4}g was from 30 to 50% lower than that measured for 1g.

Thus, both the solute boundary layer and the overall stability criterion will be affected. If D_{ef} is substituted for D in eq. (1), a simple analysis indicates that high-g should have a stabilizing influence on the interface, since the right hand term becomes smaller.

In view of the above, it seems fair to conclude that, in general, interface stability is improved by higher g levels, although in particular cases the contrary may be true.

2.2. Interphase Spacing: The interlamellar spacing in eutectic solidification is related to diffusivity by:

$$\lambda^2 R \sim D_{ef} \quad (7)$$

It follows that, since $D_{ef(hig-g)} > D_{ef(low-G)}$ also $\lambda_{hig-g} > \lambda_{low-g}$. In other words low-g solidification should result in finer eutectic structure.

2.3. Nucleation Kinetics: The influence of gravity level over nucleation kinetics can be rationalized in terms of constitutional undercooling. As shown in Fig. 6, because of the smaller δ_c in

high-g, the constitutional undercooling ΔT_{max} becomes higher, which will result in larger number of nuclei. Thus, it is expected that a low-g environment during solidification will result in decreased nucleation, i.e. coarser grains.

Another aspect related to nucleation has to do with the so called "grain multiplication mechanisms". For the case of dendritic solidification, it is rather widely accepted that convection currents in the liquid may break the tips of the dendrites, which have very little strength due to the high temperatures involved. These particles are then swept ahead of the interface by convection flow [23] and they can act as nuclei (Fig. 7). The supression of this grain multiplication mechanism under low-g has been demonstrated for transparent metal analog material [7]. Thus, the higher the convection level, the higher the number of grains, which again means that low-g solidification should result in coarser grains.

2.4. Immiscible Particle Behavior at the Interface: When a moving solidification front intercepts an insoluble particle, it can either push or entrap the particle. The existence of a critical interface rate, R_{cr}, under which particles are pushed and above which particles are entraped has been demonstrated experimentally [8]. Different theoretical avenues to explain this phenomenon have been pursued by a number of investigators [8,9,10,11]. At the present time, it is accepted that the variables governing particle behavior at the interface are: particle shape, surface energy between particle, liquid and solid, particle aggregation, thermal conductivity of solid,

liquid and particle, liquid-solid interface shape, convection level in the liquid, density of liquid and particle, and, finally, the thermal gradient.

Since the last four variables are gravity dependent, it is quite obvious that the gravity level will have a significant role in particle behavior. It has been shown that low-g has, in general, a destabilizing influence on the interface. This will favor particle entrapment rather than pushing, since particles will be easier entraped by a rough interface.

In addition to convection effects, the density difference between particles and liquid will result in Stokes forces being active on the particles. In high-g, they can work for or against entrapment, while in zero-g, they are non-existent. Thus, low-g experimentation helps eliminate one of the variables of this complicated phenomenon, and therefore is a useful tool in studying it.

3. EXPERIMENTAL METHOD

The method used in this research for studying the effects of low-g on solidification of alloys, was to have a Bridgman type directional solidification furnace, described elsewhere [12], flown on the NASA KC-135 aircraft during repetitive, parabolic, low-g maneuvers. Each maneuver gives from 20 to 30 seconds of low-g and up to 1.5 minutes of pullout and climb, as shown in Fig. 8. Therefore, a sample being solidified experiences a repetitive sequence of low-g and high-g forces parallel to the longitudinal growth axis. The acceleration experienced by the sample was monitored by three

accelerometers mounted to the furnace assembly. For a typical maneuver during low-g, the acceleration on all axes averaged around 10^{-2}g. It was found that for the NH_4Cl-H_2O metal analog system macro-convective flow stopped within 8 seconds during a low-g maneuver [13]. During pullout and climb, the high-g acceleration parallel to the longitudinal axis of the sample reached 1.75g, while the accelerations on the other two axes were less than 0.15g. The known solidification rate of the sample can then be correlated with accelerometer data to determine the gravity level during solidification for any location on the sample.

For most of the flight experiments, an equivalent ground experiment (1g control sample) was run at the same growth rate (R), furnace thermal gradient (G), and other experimental conditions.

4. NUCLEATION AND GRAIN MULTIPLICATION IN Fe-C ALLOYS

In one of the first experiments performed using the technique described above, a laboratory purity Fe-C-Si-P alloy (4.33%C, 1.53%Si, 0.1%P, 0.052%Mn, 0.011%S) was used. Phosphorus was purposely added to allow for easy metallographic determination of eutectic grains. As shown in Fig. 9, the number of eutectic grains decreased with every transition from high-g to low-g. The points on the figure represent the average count for each zone. When the variation of eutectic grain count was plotted within the high-g/low-g zones for a sample of commercial composition (Fig. 10), it was found that the number of grains decreased along the low-g zone and increased along the high-g zone. No significant change in the number of eutectic grains was found on the control (ground) sample.

As discussed in paragraph 2.3, this is rationalized in terms of lower constitutional undercooling in low-g, but it must be noted that the absence of some grain multiplication mechanism, which is active in high-g, cannot be ruled out. In other words, natural convection in high-g can influence either directly, by a grain multiplication mechanism, or indirectly, by increasing constitutional undercooling.

Experiments are presently run in order to assess quantitatively the contribution of natural convection during high-g solidification to the final number of eutectic grains for both inoculated and uninoculated samples [14]. For experiments with no inoculation, the final number of eutectic grains is:

$$N_{high-g} = N_h + N_c \tag{8}$$

while for experiments with inoculation it becomes:

$$N_{high-g(i)} = N_h + N_{ih} + N_C \tag{9}$$

where N_h: number of grains resulting from heterogeneous nucleation

N_{ih}: number of grains resulting from induced heterogeneous nucleation (contribution of inoculation)

N_c: number of grains resulting from contribution of convection

For low-g experiments, it can be assumed that:

$$N_{low-g} = N_h \tag{10}$$

and

$$N_{low-g(i)} = N_h + N_{ih} \tag{11}$$

By manipulating eq. (8) through (11), information can be obtained on various factors influencing nucleation. For example, subtracting eq. (10) from (8) allows quantitative determination of N_c.

Some preliminary experimental results are shown in Fig. 11. Interpretation of these results as described above, allows for calculation of an approximate 19% increase in the number of nuclei due to convection in high-g as compared with low-g.

It is quite obvious that while the DSPT technique can give useful results, definitive results can only be obtained by shuttle experiments.

5. INTERFACE STABILITY IN Fe-C ALLOYS

Again, alloys solidifying in the stable Fe-C system have been used to experimentally evaluate the influence of low-g on interface stability. Figures 12 and 13 show good evidence of destabilization of interface upon transition from high-g to low-g zones [12], which is in agreement with the theoretical analysis in paragraph 2.1. Similar behavior has been observed on a Mo-Ni-Ni_3Al monovariant eutectic alloy during the DI mission [22].

6. INTERPHASE SPACING IN Fe-C ALLOYS

Since the Fe-Graphite eutectic is an irregular lamellar eutectic, measurements of interlamellar spacing in such an alloy are rather difficult. Accordingly, metastable Fe-C alloys (white iron) were chosen for these experiments. Figure 14 shows that the interlamellar spacing decreases sharply along the low-g zones, while increasing in

the high-g zones, which amounts to a refinement of the interlamellar spacing in low-g. This is in line with the concept of effective diffusivity formalized in eq. (7).

Some interesting effects of low-g were also observed on the secondary dendrite arm spacing (SDS) on both commercial and high purity composition Fe-C-Si alloys. The SDS decreased during the high-g zones, but increased during the low-g zone (Fig. 15), i.e. dendrites were refined during solidification in high-g zones, but were coarsened along the low-g zones. Similar results were reported on superalloys for SDS in ref. [15] and for primary dendritic spacing in ref. [16].

7. INSOLUBLE PARTICLES BEHAVIOR AT THE LIQUID/SOLID INTERFACE

Three different systems were investigated, as follows: Fe-C alloys in the Fe-spheroidal graphite system, in-situ composites in the Fe-VC system and metal matrix composites in the Al-SiC system.

7.1. The Iron-Spheroidal Graphite System: This is a system of significant practical importance in metal casting, the material being known as spheroidal graphite (SG) cast iron. When a hypereutectic alloy is considered, graphite is the primary phase and SG separates in the liquid prior to eutectic solidification. Thus, SG can be viewed as an immiscible particle and the whole system as an in-situ composite. To achieve the desired structure, Ce was added to a base Fe-C-Si alloy [12]. The structure of this alloy was white (i.e. exempt of graphite) before remelting in the directional solidification furnace, and gray (i.e. graphite + austenite) after resolidification.

Two different effects occur in conjunction with low-g processing during solidification, as follows: (1) flotation of graphite spheroids (since the samples were solidified upward) and (2) change in the fineness of the eutectic structure (change in the number of graphite spheroids).

Indeed, DSPT samples exhibited banding of graphite spheroids of larger size than that typical of the rest of the sample. Although those bands were not always positioned over the low-g zones, they are explained by supression of graphite flotation in the low-g zones. Since theromdynamic considerations (phase equilibria) predicts graphite entrapment in the iron matrix, it is not surprising that large graphite spheroids are entraped together with small spheroids in the low-g zone. Superimposing flotation rate and growth rate over a variable g field predicts this type of banding [17].

The influence of low-g processing on the graphite spheroid count is shown in Fig. 15. During the first low-g zone shown in the graph, the number of graphite spheroids decreases and increases again in the subsequent high-g zone. This phenomenon can be explained again in terms of constitutional undercooling (Fig. 5). The data on the second low-g zone are less significant, since in that particular zone, solidification caught up with flotation resulting in a mixed structure of fine and coarse graphite spheroids.

7.2. The Fe-VC System: One of the main difficulties expected in the manufacturing of dispersed carbides in-situ composites by casting techniques, is to obtain a uniform distribution of carbides in

the matrix. Non-uniform distribution can result from buoyancy effects and from the behavior of carbide particles at the moving solid-liquid interface.

The Fe-VC system is not only a good model system but is, again, a system with commercial significance, since, for example, a 12%V cast iron has considerably higher wear resistance properties than high chromium cast iron.

A number of Fe-C-V samples were processed by DSPT. Their composition was such as to be hypereutectic, which resulted in primary VC particles separating from the liquid. Experiments done on Fe-C-13%V alloys have shown that for growth rates of 4.95 mm/min, VC particles were entraped in the low-g regions, but floated out of the high-g regions (Fig. 17) [18], which was in line with Stokes velocity calculations for VC particles in molten iron [19].

In order to try to achieve a uniform VC distribution without having to resort to space processing, Fe-C-10.7%V samples were DS in directions parallel (downward), antiparallel (upward) and perpendicular (horizontal) to the gravity vector. As shown in Fig. 18, the only way to obtain a uniform composite was by solidifying downward [20]. Unfortunately, three dimensional castings can not be produced that way, which points to space processing as the only viable alternative.

The size of primary particles, in this case VC, decreases at high-g/low-g transtions or within the low-g region (Fig. 19). Since the growth rate is diffusivity dependent, i.e. $R \sim D_{ef}$, it follows that $R_{low-g} < R_{high-g}$ which would result in

smaller VC particles in low-g as compared to high-g. Also, it was again confirmed that, as in the case of the Fe-graphite eutectic, the distribution of VC particles in the flight samples occurs as bands.

The formation of VC rich zones in samples run under variable gravity levels at growth rates higher than Stokes velocity, indicates that some interaction between VC particles and the solid-liquid interface cannot be ruled out. VC particles were probably pushed when Stokes forces were absent, but there cannot be any conclusive proof of this, unless solidification is run under completely low-g conditions as in the space shuttle.

7.3. The Al-SiC System: Metal matrix composites in the Al-SiC system are now available commercially. Nevertheless, since these alloys are good model systems for the study of particle behavior ahead of the solid-liquid interface, experiments were conducted to verify the concept of critical rate for particle entrapment, R_{cr}, [21] as well as to asses the general influence of low-g processing on SiC particle behavior.

About 10% by weight silicon carbide particles, ranging in size from 2 to 100 μm, were dispersed in Al-2%Mg alloys by casting techniques. In the ground experiments summarized in Table 2, it was, indeed, confirmed that by increasing the growth rate at a given temperature gradient, or by decreasing the gradient at a given rate, the behavior of particles is changed from pushing to entrapment. This is a direct experimental confirmation of the theoretical work in ref. [8]. Some good uniform structures were produced, as shown in

Fig. 20. The only unexpected result was pushing of particles larger than 20μm, while particles smaller than 20μm were entraped (sample 4, Table 2), while theoretically $R_{cr} \sim 1/r^n$, where r is the particle radius. This means that large particles should be entraped before small particles. It must be noted though that while this is true for planar interfaces, the situation may be different when the interface becomes unstable. Indeed, as shown in Fig. 21, the interface of Al-SiC composites is quite unstable, to be more precise, cellular and subcellular in this particular case. As the growth rate increases, the interface can even become dendritic and then big particles can be pushed by the tips of the dendrites while small particles are entraped (Fig 22).

A summary of the results of flight experiments is given in Table 3. Besides confirming the ground results on the qualitative correlation between R_{cr}, G and particle behavior, it can be seen that decreasing the g level seems to favor particle pushing over particle entrapment. In other words, the force pushing the particles into the interface decreased with gravity.

The drag force over a particle, is given by [8]:

$$F_d = \frac{6\pi\eta r^2 R}{d} \qquad (12)$$

where η: viscosity of the liquid

d: minimum gap between particle and solid, resulting from repulsion by molecular forces

Apparently, none of the parameters influencing F_d is gravity dependent. The total force pushing the particle in the interface is:

$$F_p = F_d + F_s \qquad (13)$$

where F_s: Stokes force; can be positive or negative.

In the case of the Al-SiC system, F_s is positive, that is SiC particles are denser than the liquid and tend to settle. This means that F_d and F_s are additive. When solidifying in low-g, F_s tends to zero, which results in a smaller F_p.

8. CONCLUSIONS

On the theoretical side, it can be concluded that low-g solidification lowers interface stability and interlamellar spacing in eutectics while coarsening the secondary dendrite arm spacing. As expected, sedimentation or flotation of immiscible particles is decreased in low-g and can be prevented under micro-g conditions.

On the practical side, low-g solidification allows for production of metal matrix composites in tri-dimensional shapes, regardless of the relative densities of particles and liquid. Most of the experiments discussed in this paper require longer low-g periods (e.g. shuttle) for definitive confirmation.

While waiting for shuttle flights or for the space station to materialize, DSPT is a viable experimental method which can provide qualitative and semiquantitative answers.

Acknowledgements

The research work summarized in this paper has been made possible through grants to the Department of Metallurgical Engineering at The University of Alabama from various organizations which are listed here in alphabetical order: Center for Space Processing of Engineering Materials (Vanderbilt University), General Motors, John Deere & Company and NASA.

The authors are grateful to Profs. J. Berry and B. Dhindaw as well as Dr. I. G. Chen for helpful discussions during the preparation of the manuscript.

References

1. Challenges and Prospectives of Microgravity Research in Space, (European Space Agency Rep. BR-05, 1981).
2. R. Jansen and P. R. Sahm, Materials Science and Engineering, 65 (1984), 199.
3. M. C. Flemings, Solidification Processing, (McGraw-Hill, 1974).
4. J. A. Burton, R. C. Prim and W. P. Slichter, J. Chem., 21 (1953) 1987.
5. G. Frohberg, in: Materials Science in Space, B. Feuerbacher, N. Hamacher, R. J. Naumann, (Springer-Verlag, 1986), 91.
6. G. Frohberg, K-H. Kraatz and H. Wever, in: 5th European Symposium on Materials Sciences under Microgravity-Results of Spacelab-1, (Schloss Elmau FRG, Nov., 1984), 201.
7. M. H. Johnston, C. S. Griner, R. A. Parr and S. J. Robertson, J. Crystal Growth, 50 (1980), 831.
8. D. R. Uhlmann, B. Chalmers and K. A. Jackson, J. Appl. Physics, 35 (1964) 2986.
9. A. A. Chernov, D. E. Temkin and A. M. Melinkova, Sov. Phys. Crystallogr., 21 (1976) 369.
10. G. F. Bolling and J. Cissé, J. of Crystal Growth, 10 (1971) 56.
11. S. N. Omenyi and A. W. Neumann, J. Appl. Physics, 47 (1976) 3956.
12. D. M. Stefanescu, P. A. Curreri and M. R. Fiske, Met. Trans., 17A (1986) 1121.

13. M H. Johnston and R. B. Owen, Met. Trans., 14A (1983) 2163.

14. S. K. Biswal and D. M. Stefanescu, BER Report No. 401-202 to John Deere & Co., (The University of Alabama, 1987).

15. M. H. Jonston, P. A. Curreri, R. A. Parr and W. S. Alter, Met. Trans., 16A (1985) 1683.

16. M. H. McCay, J. E. Lee and P. A. Curreri, Met. Trans., 17A (1986) 2301.

17. J. C. Hendrix, P. A. Curreri and D. M. Stefanescu, Trans. of American Foundrymen's Soc., 99 (1984) 435.

18. D. M. Stefanescu, M. R. Fiske, and B. Dhindaw, BER Report No. 382-202 to NASA (The University of Alabama 1986).

19. D. M. Stefanescu, M. R. Fiske and P. A. Curreri, in: 18th International SAMPE Conference, 18 (1986) 309.

20. B. K. Dhindaw, D. M. Stefanescu, P. A. Curreri and D. K. Bandyopadhyay, Solidification Processing, Sheffield (1987), in print.

21. B. K. Dhindaw, A. S. Kacar and D. M. Stefanescu, in: First ASM-Europe Conference, Paris, (1987) in print.

22. H. J. Sprenger, in: Sixth European Symposium on Materials Sciences under Microgravity Conditions (Europena Space Agency, Paris, 1987) 349.

23. M. Simson and M. Flemings, Met. Trans., 15A (1984) 2095.

LIST OF FIGURES

13. Transition from cellular solidification (type A graphite) to equiaxed solidification (type D graphite and eutectic grains) at a high-g/low-g transition on a commercial Fe-C-Si-P alloy. Nital etched, 46X [12].

14. Variation of the interlamellar spacing of the Fe-Fe_3C eutectic on a sample processed by DSPT. R = 5.17 mm/min [12].

15. Variation of secondary dendrite arm spacing for austenite in a pure Fe-C-Si alloy processed by DSPT. R = 4.89 mm/min [12].

16. Variation of number of graphite spheroids along a sample of commercial composition Fe-C-Si-Ce alloy processed by DSPT. R = 2 mm/min [12]

17. Microstructures of Fe-C-13.18%V samples, 100 X: a) Ground DS - colony structure, very few VC particles; b) DSPT processed - VC carbides in 3rd low-g region [18].

18. Microstructures of Fe-C-10.7%V ground samples: a) DS upward, 100 X; b) DS horizontally, 100 X; c) DS downward, 200X [20].

19. Variation of VCparticle size along a DSPT processed sample [20].

20. Structure of a DS sample showing good distribution of SiC particles in an Al-2%Mg matrix, 7 X.

21. Pushing of big particles (agglomerate) by the tip of the dendrites in an Al-SiC sample, 50 X.

22. Quench interface of an Al-SiC sample showing cellular and subcellular structure, 50 X.

TABLE I: Correlation between Convenction Level, Gravity Level δ_c and k_{ef}

Convection level	Gravity level,g	δ_c	k_{ef}
~zero	g=0	large	1
moderate	0<g<1	moderate	$k<k_{ef}<1$
high	g=1	zero	$k_{ef}=k$

Table II: Summary of Ground Experiments with Al-SiC Composities

Sample No.	Temperature Gradient, °C/cm	SiC particle size, μm	Growth rate, mm/min	Particle Behavior
1	74	2 - 100	0.48	Entraped
2	95	50 - 100	0.48	Pushed/Entraped*
3	95	50 - 100	24.0	Entraped/Pushed**
4	117	2 - 100	0.48	Particles >20μm Pushed Particles <20μm Entraped
5	117	50 - 100	4.8	Pushed/Entraped

* i.e. particles were pushed for some distance, but when the volume of particles built up, particles were entraped.

** i.e. pushing for short distances

Table III: Summary of Results of Ground and DSPT Processing.
R = 4.8 mm/min

Temperature Gradient, °C/cm	Solidification Processing	Particle Behavior
74	Ground (1g)	Entrapment
74	DSPT (high-g/low-g)	Pushing/Entrapment
117	Ground (1g)	Pushing/Entrapment
117	DSPT (high-g/low-g)	Pushing

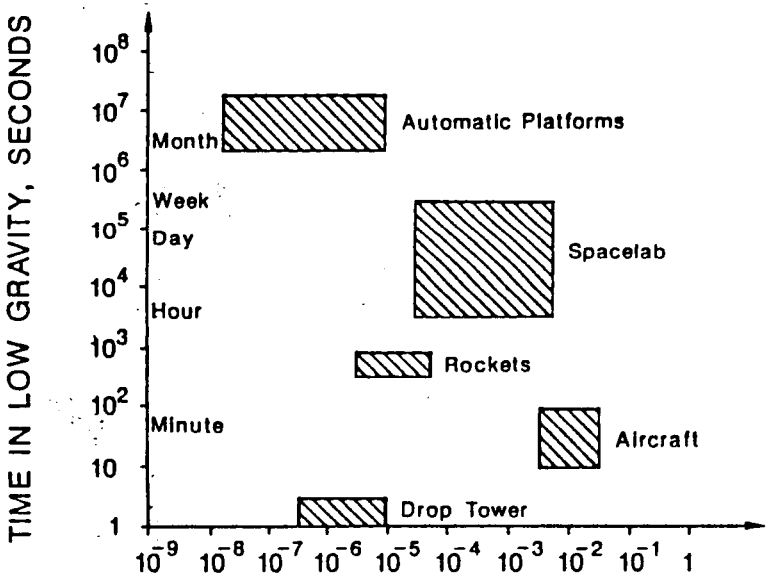
TIME IN LOW GRAVITY, SECONDS
10^8
10^7
Month
10^6
Week
10^5
Day
10^4
Hour
10^3
10^2
Minute
10
1
Automatic Platforms
Spacelab
Rockets
Aircraft
Drop Tower
10^{-9} 10^{-8} 10^{-7} 10^{-6} 10^{-5} 10^{-4} 10^{-3} 10^{-2} 10^{-1} 1
GRAVITY LEVELS, g

Fig. 1

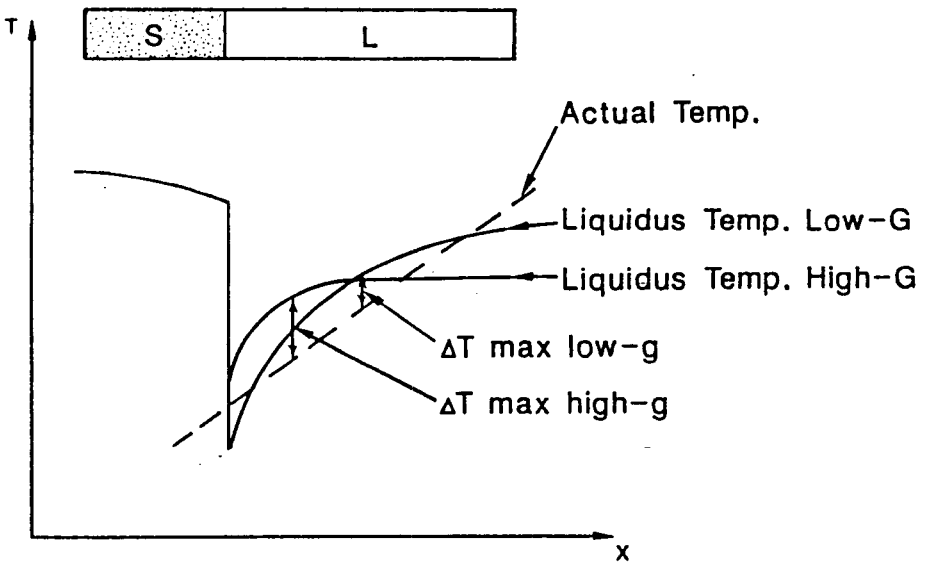
T
S
L
Actual Temp.
Liquidus Temp. Low-G
Liquidus Temp. High-G
ΔT max low-g
ΔT max high-g
x
ΔT max high-g > ΔT max low-g

Fig. 6

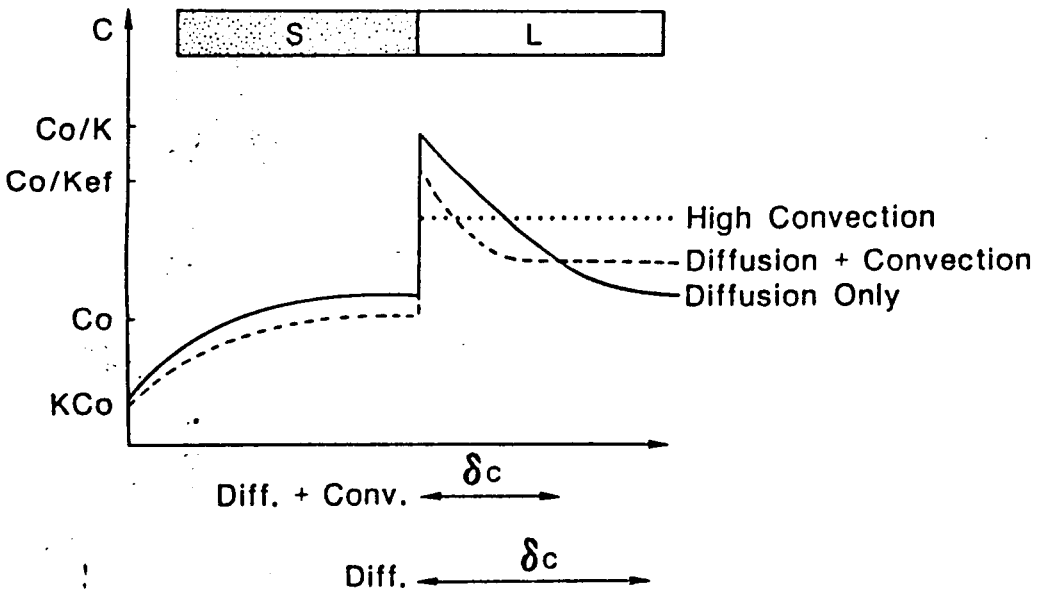
C
S
L
Co/K
Co/Kef
Co
KCo
High Convection
Diffusion + Convection
Diffusion Only
Diff. + Conv.
δc
Diff.
δc

Fig. 3

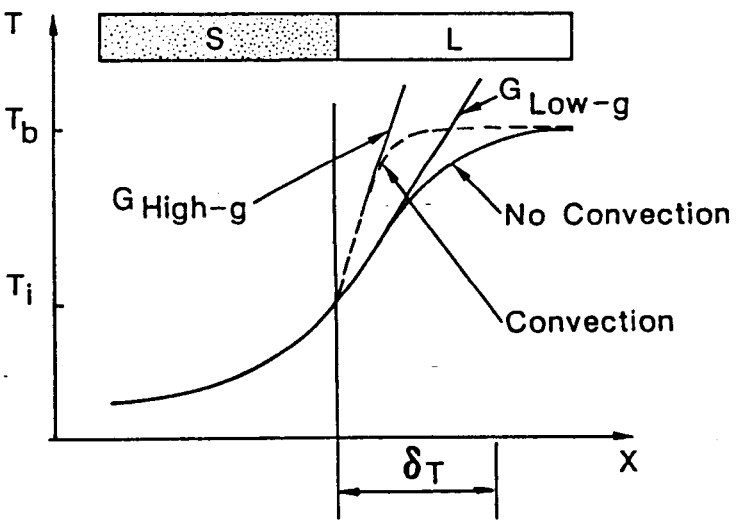
T
S
L
G Low-g
Tb
G High-g
No Convection
Ti
Convection
δT
X

Fig. 2

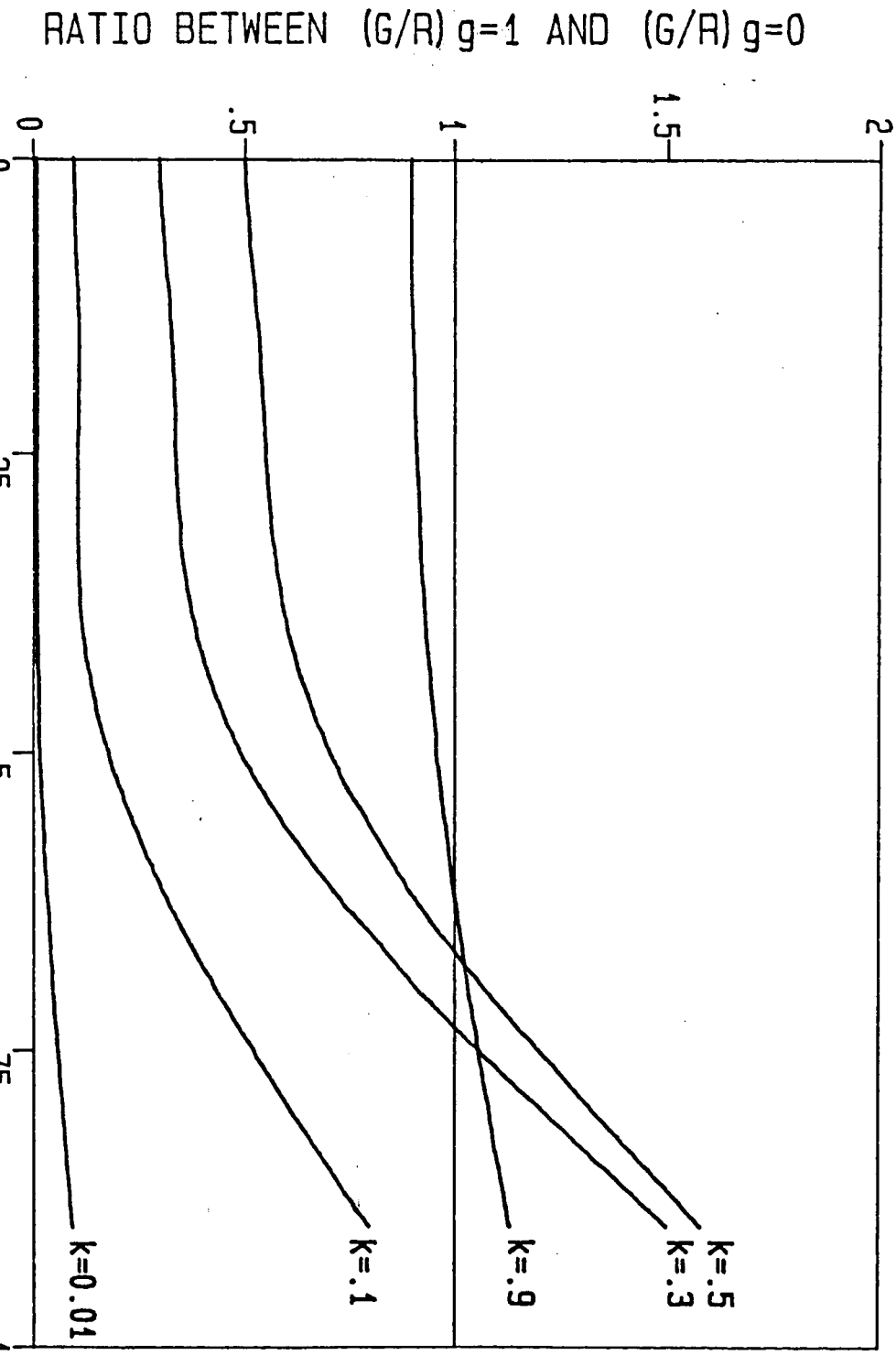

Figure 4: Ratio between G/R in low and high-g as a function of fraction of solid, f_s for different partition coefficients, k.

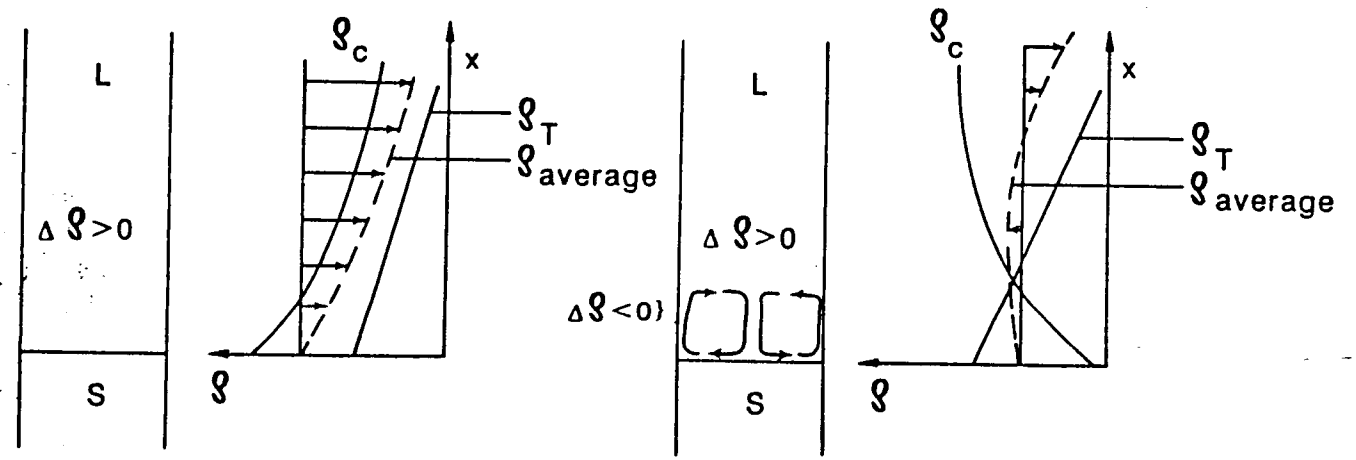

STABLE

UNSTABLE BOUNDRY LAYER
(convection)

$\Delta\vartheta = \vartheta_x - \vartheta_{x+1}$

Fig. 5

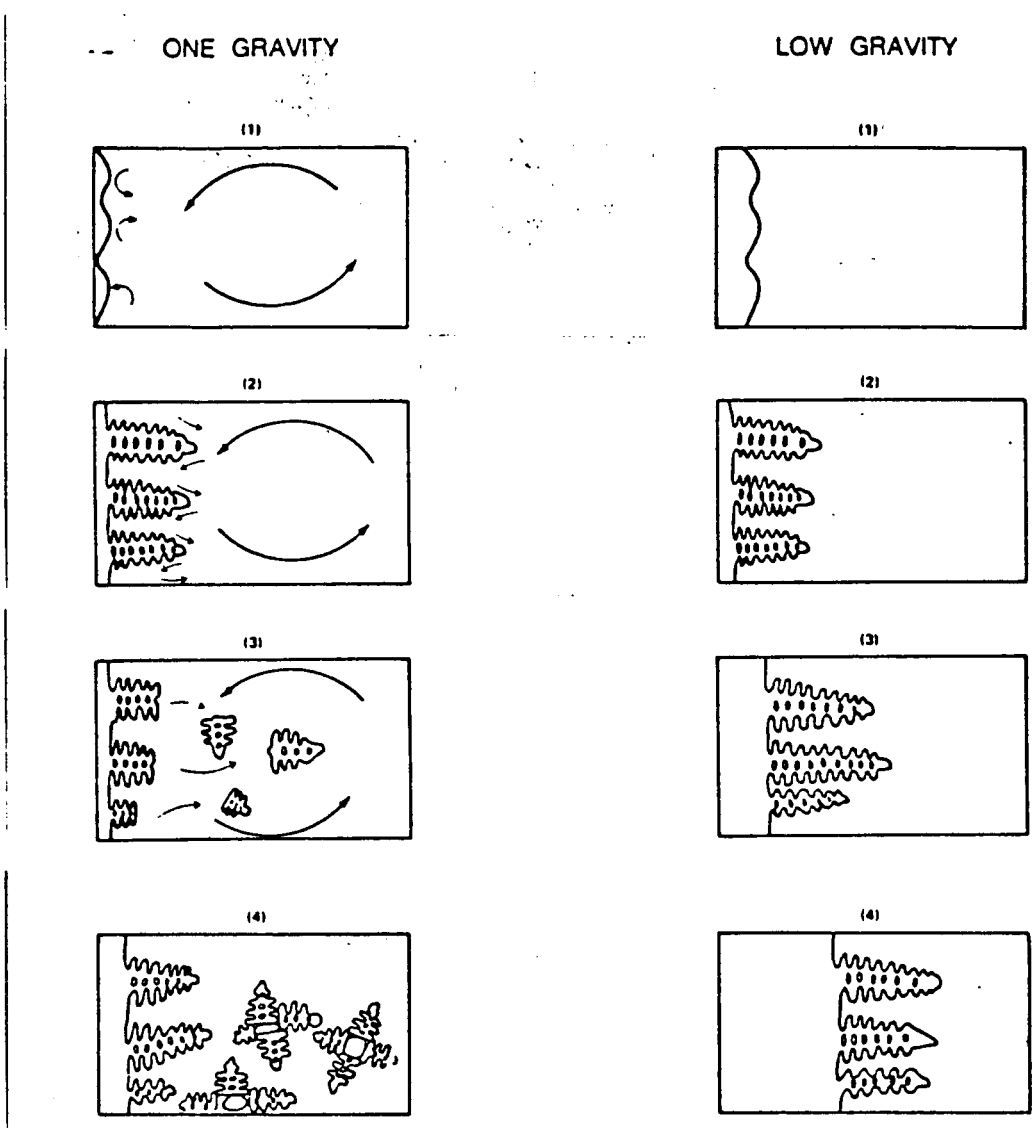

Figure 7: Possible grain multiplication mechanism in dendritic solidification.

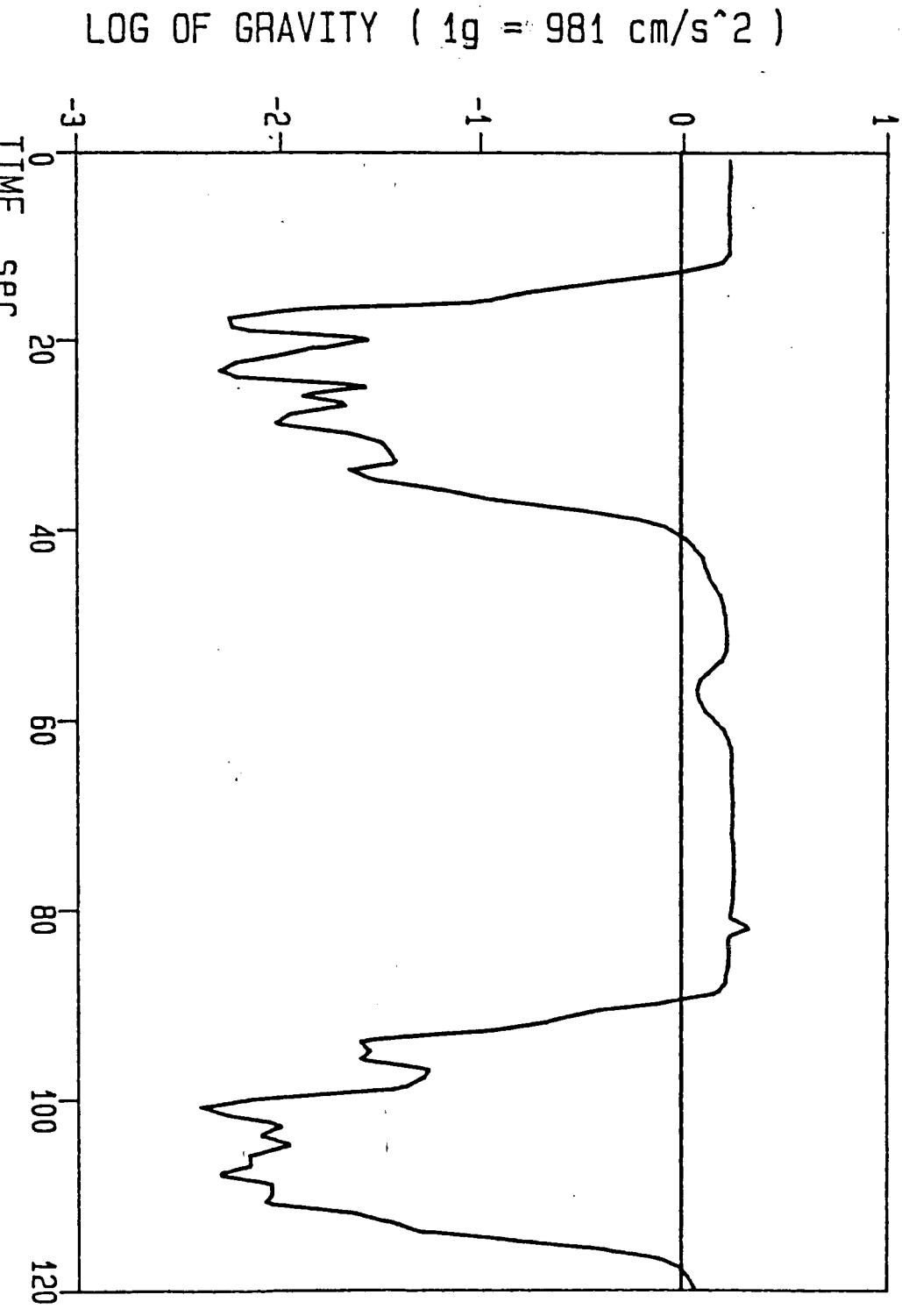

Figure 8: Typical gravity variation with time during a parabolic flight.

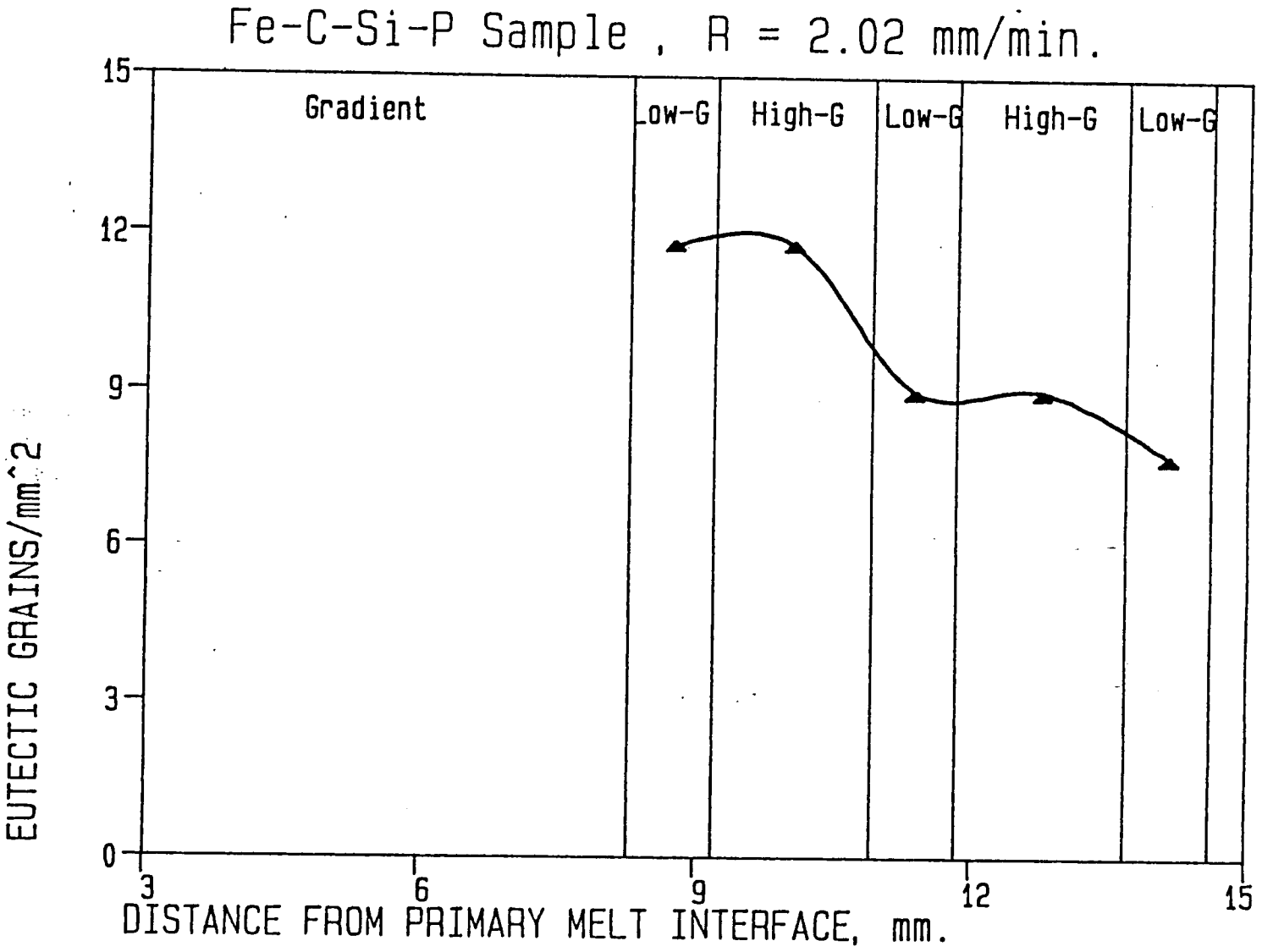

Figure 9: Variation of eutectic grain count of the austenite-flake graphite eutectic on a commercial composition Fe-C-Si-P alloy. R = 2.02 mm/min [10].

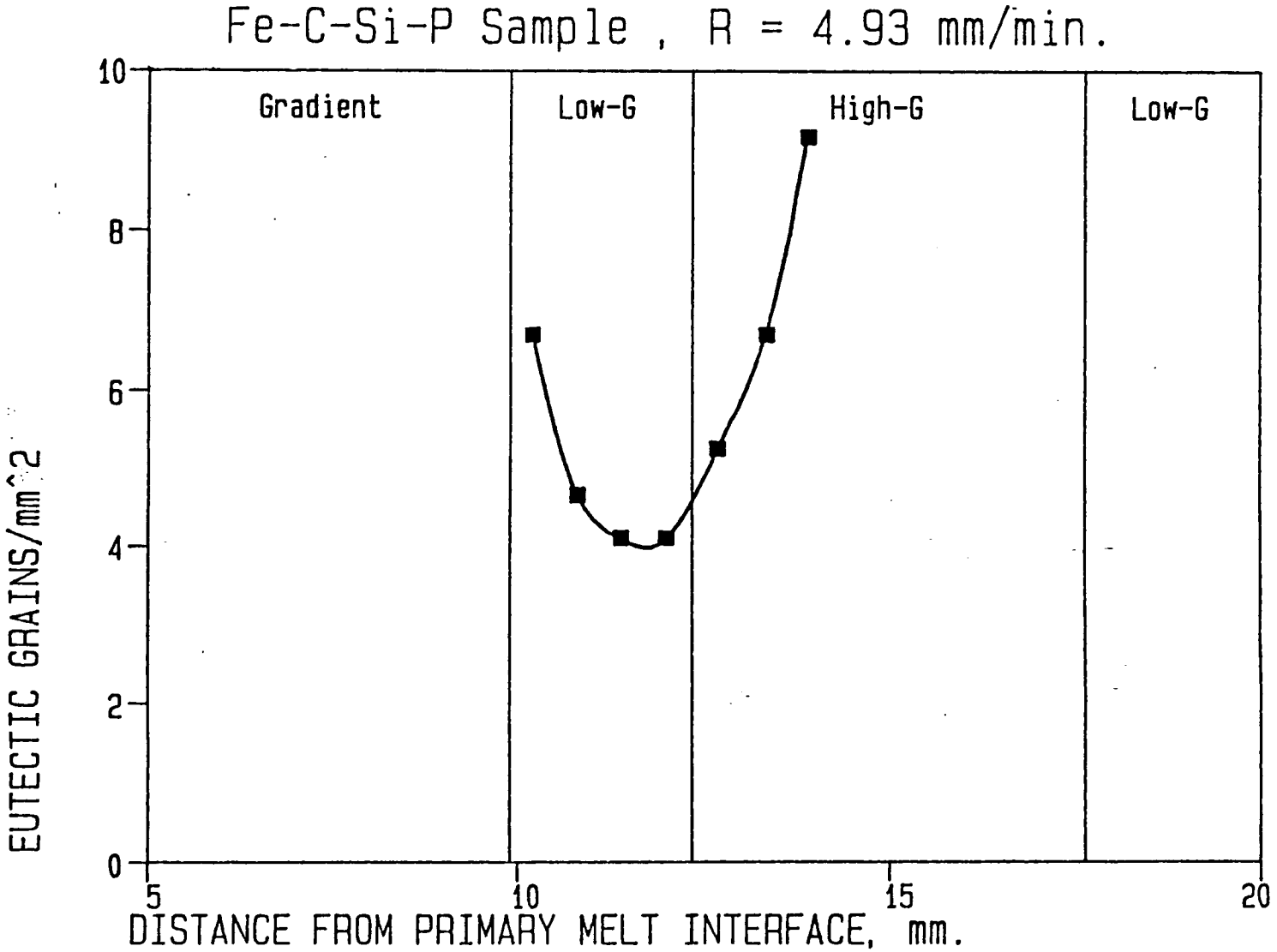

Figure 10: Variation of eutectic grain count of the austenite-flake graphite eutectic on a commercial composition Fe-C-Si-P alloy. R = 4.93 mm/min [10].

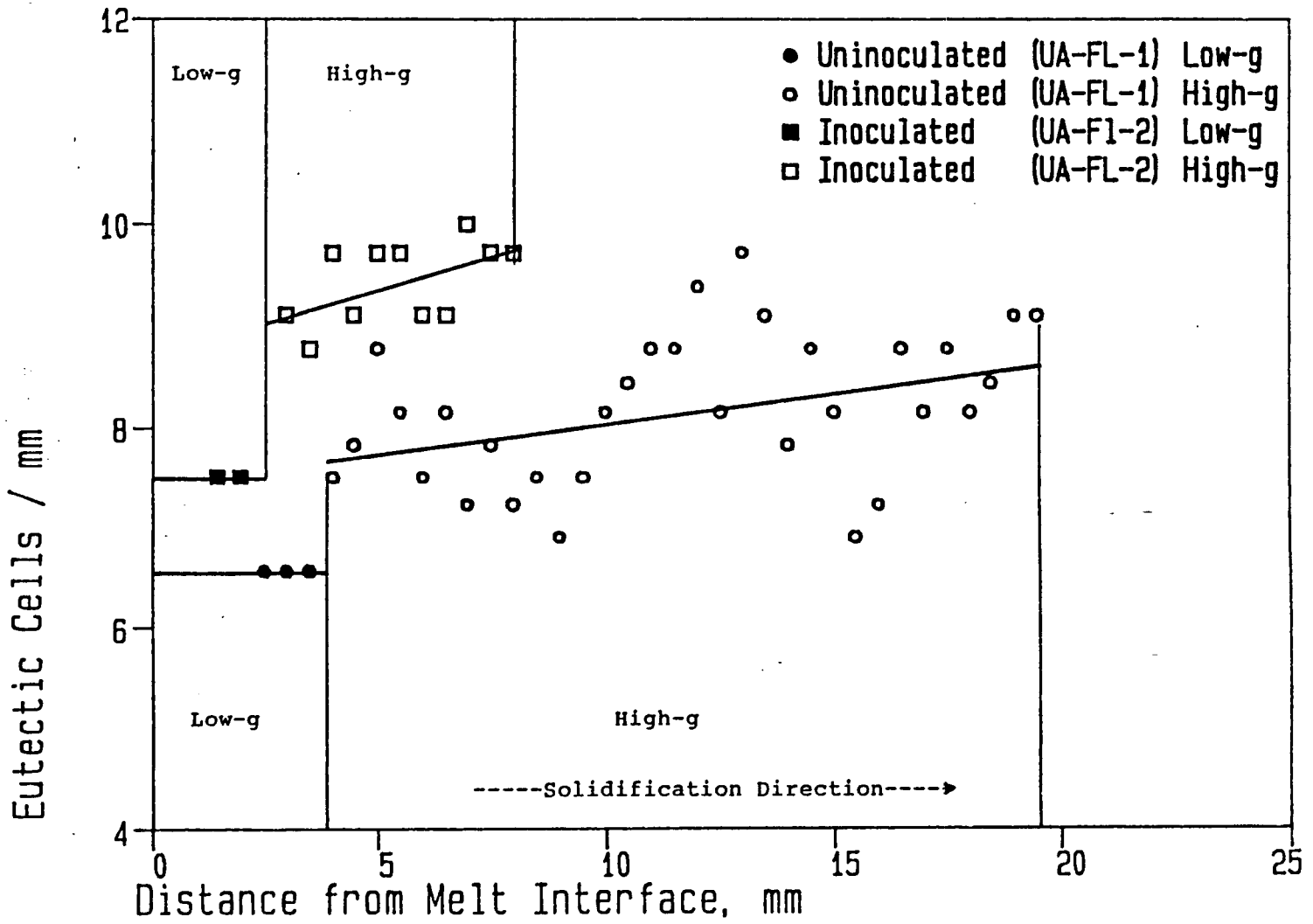

Figure 11: Eutectic grain count in inoculated and uninoculated Fe-C-Si samples processed by DSPT (transverse inoculant insert).

Fe-C-Si Alloy
Flight Sample P-2, R = 4.89 MM/min.

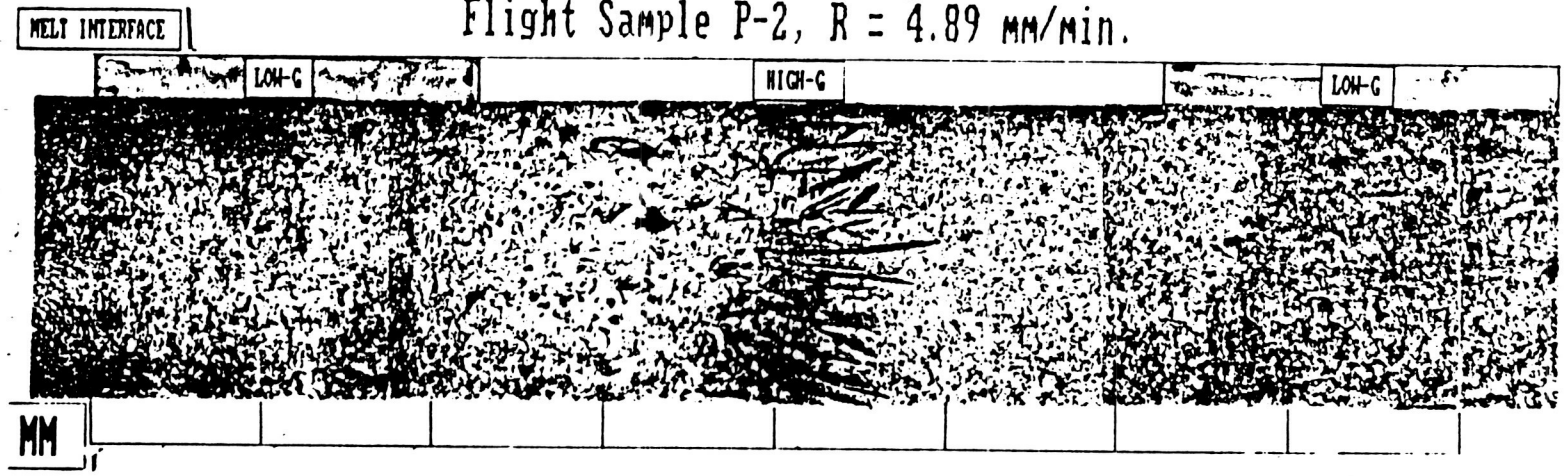

Fig 12

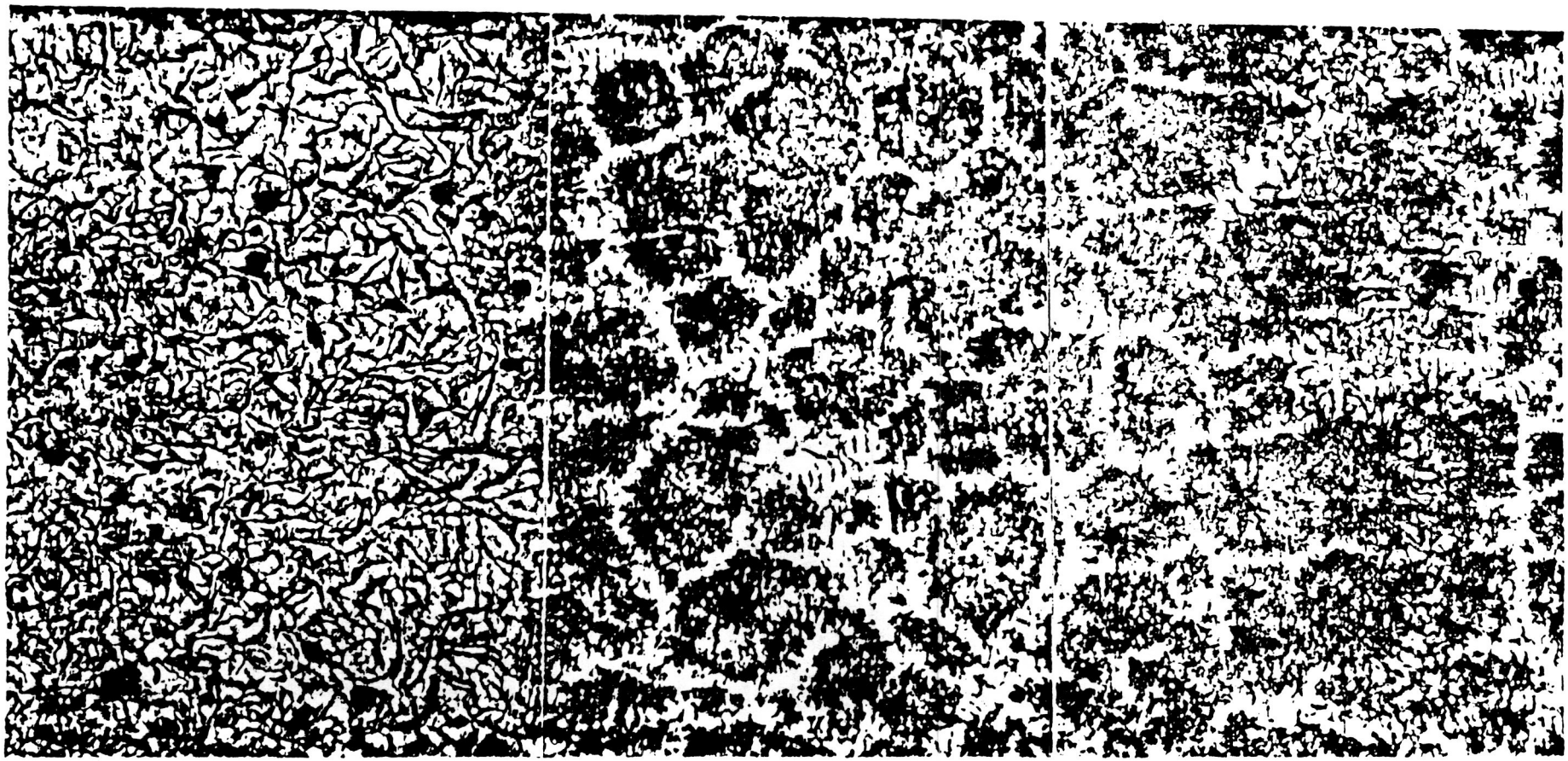

HIGH G | LOW G | HIGH G

Fig. 13

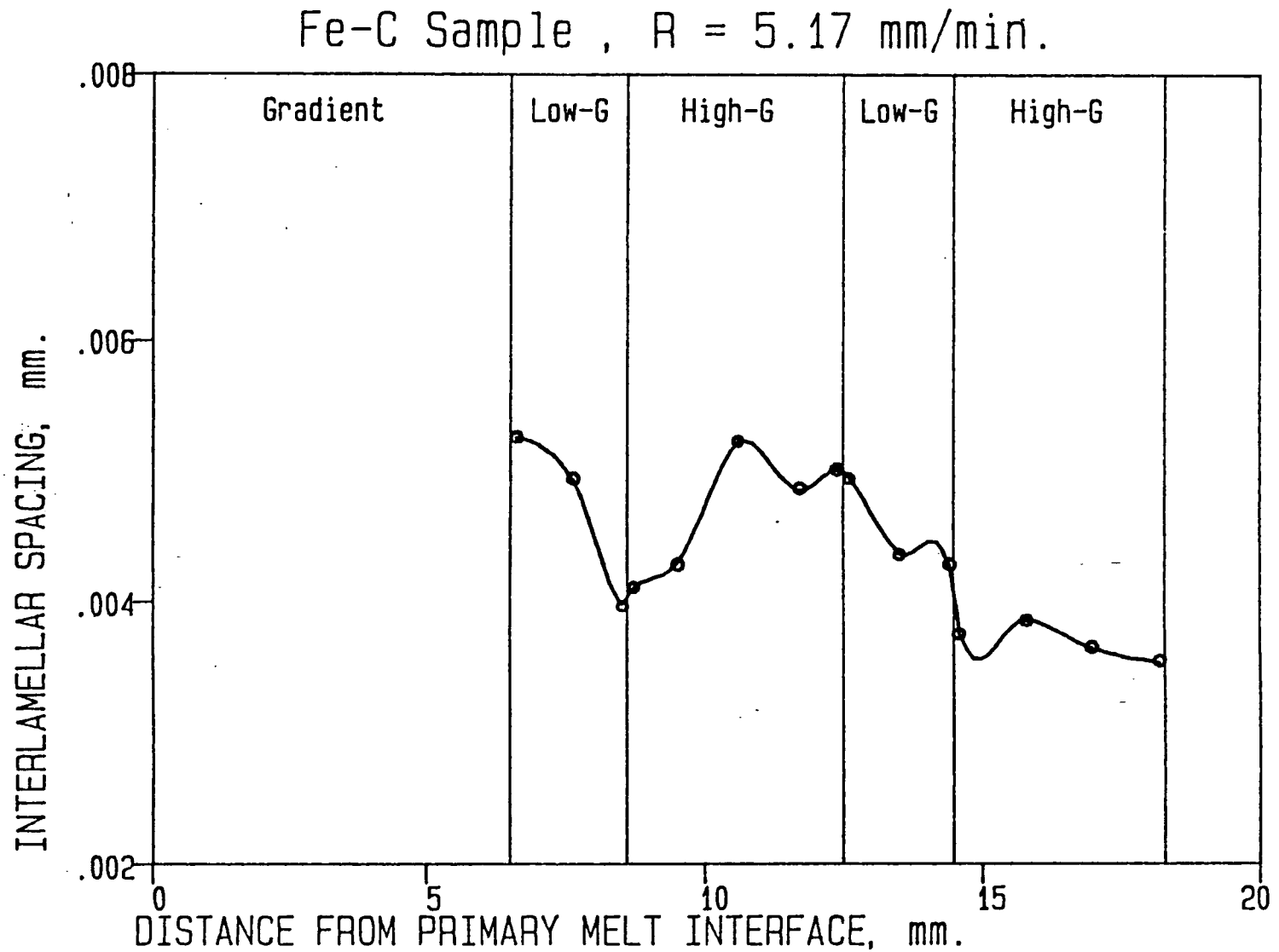

Figure 14: Variation of the interlamellar spacing of the Fe-Fe_3C eutectic on a sample processed by DSPT. R = 5.17 mm/min [10].

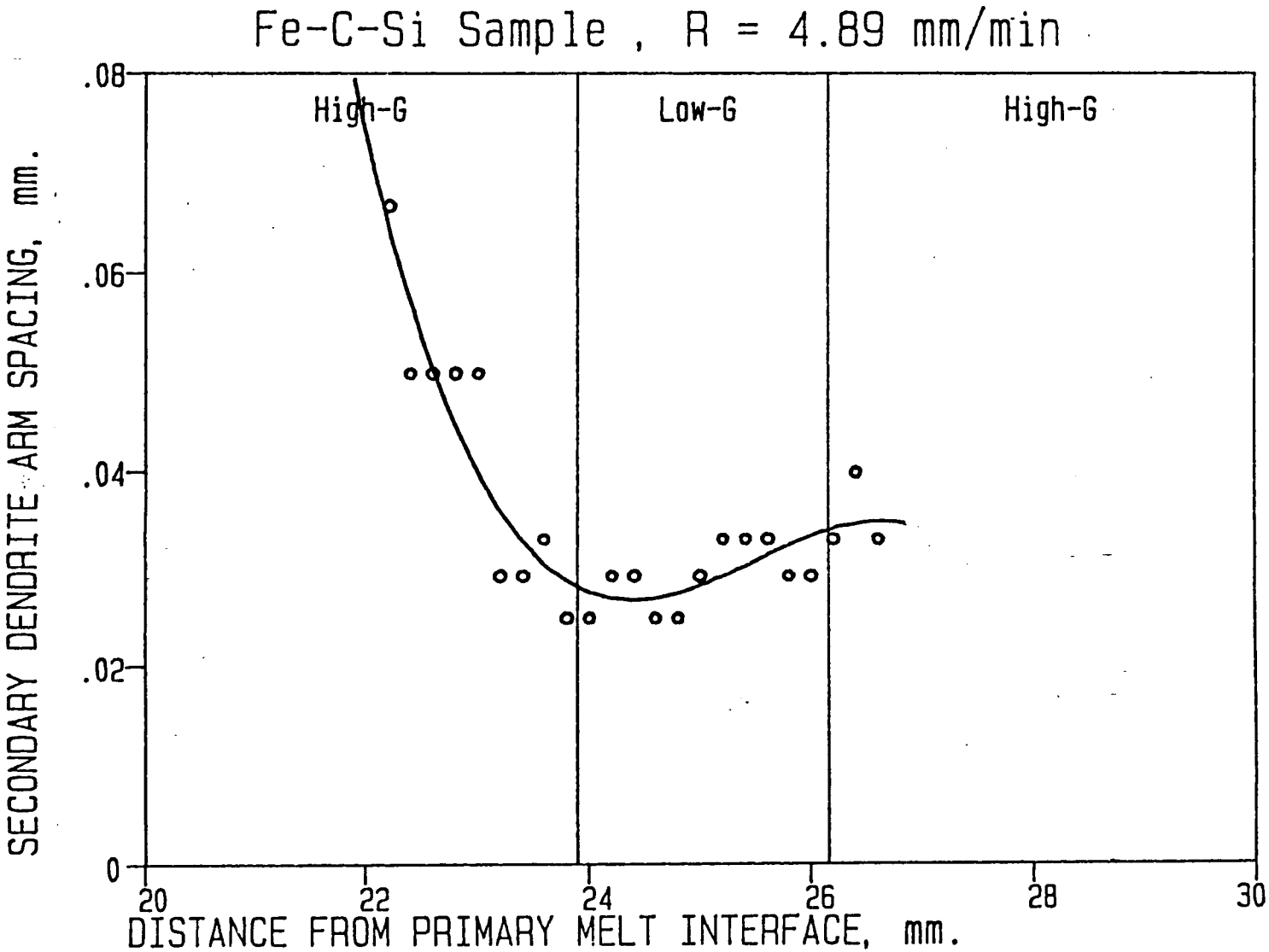

Figure 15: Variation of secondary dendrite arm spacing for austenite in a pure Fe-C-Si alloy processed by DSPT. R = 4.89 mm/min [10].

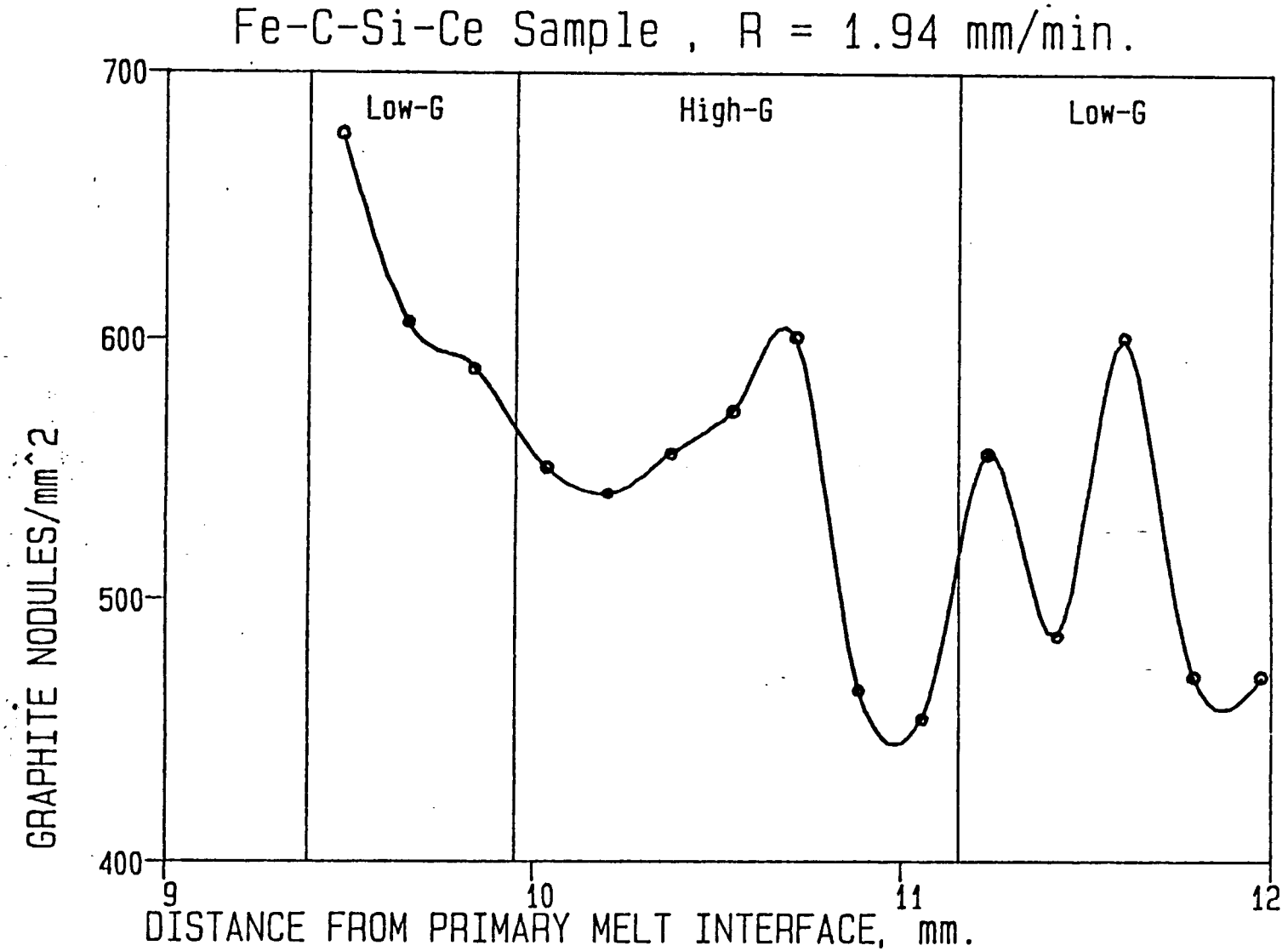

Figure 16: Variation of number of graphite spheroids along a sample of commercial composition Fe-C-Si-Ce alloy processed by DSPT. R = 2 mm/min [10].

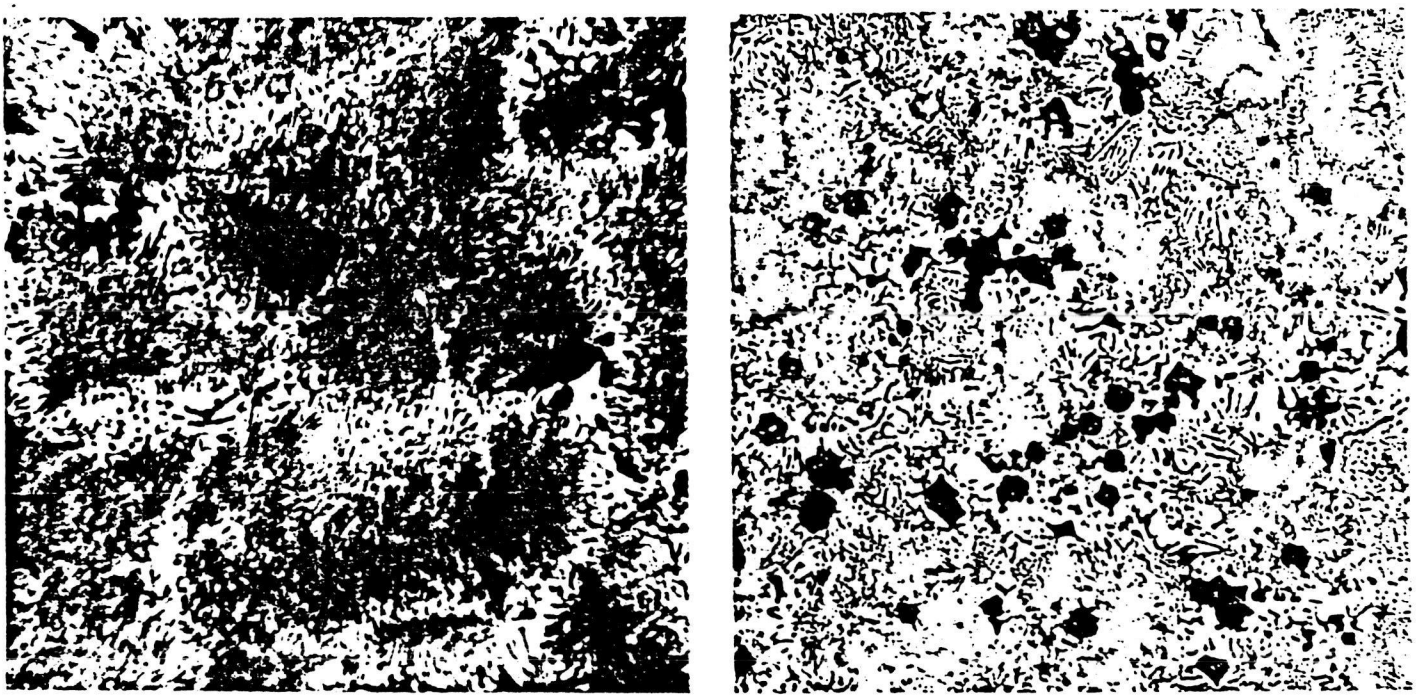

a)

b)

Fig. 17

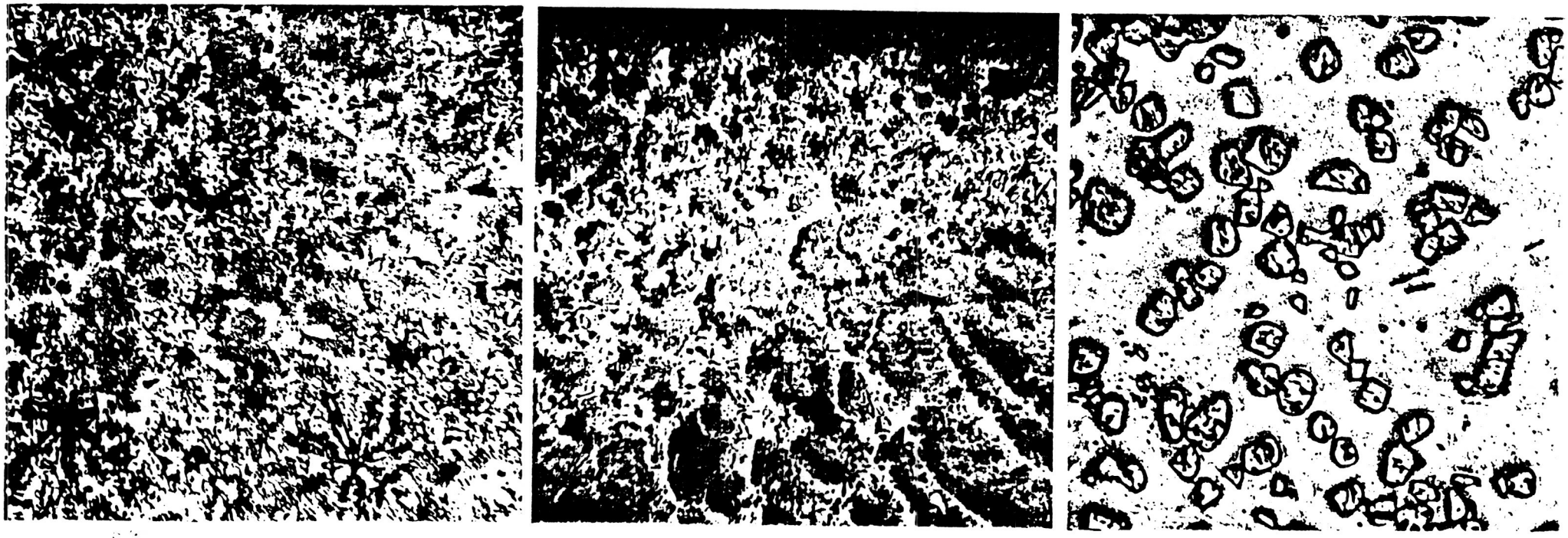

a) b) c)

Fig. 18

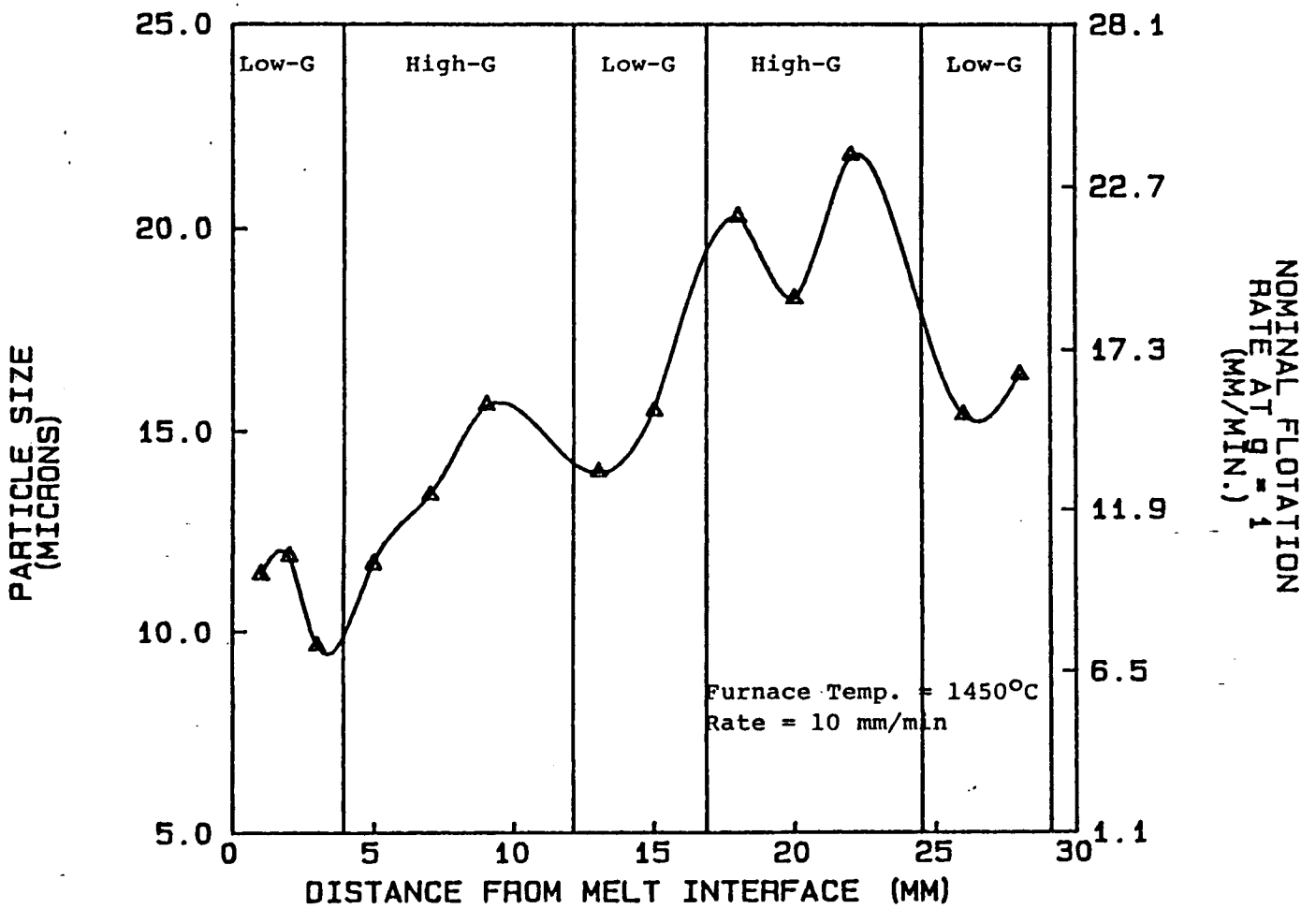
25.0
20.0
15.0
10.0
5.0
Low-G
High-G
Low-G
High-G
Low-G
28.1
22.7
17.3
11.9
6.5
1.1
Furnace Temp. = 1450°C
Rate = 10 mm/min
0
5
10
15
20
25
30
DISTANCE FROM MELT INTERFACE (MM)
PARTICLE SIZE (MICRONS)
NOMINAL FLOTATION RATE AT g = 1 (MM/MIN.)

Fig. 19

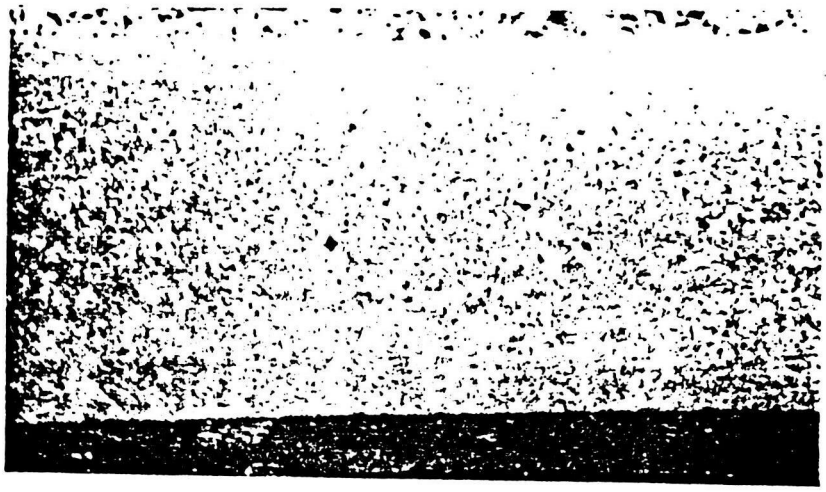

Fig. 20

Fig. 21

Fig. 22